Research Article

Structural Behavior Analysis of Rail-Mounted Portal Cranes Equipped with a 360° Rotatable Spreader Mechanism Using the Finite Element Method

Samet Dönerkaya[1*], Kemalettin Kök[2], Muhammed Emin Tamer[3]

[1] BVS Cranes R&D Center, Orcid ID: https://orcid.org/0000-0001-7577-5124, s.donerkaya@bvs.com.tr
[2] BVS Cranes R&D Center, Orcid ID: https://orcid.org/0009-0001-8690-1568, kok@bvs.com.tr
[3] Atılım University, Orcid ID: https://orcid.org/0000-0002-5228-926X, tamer@tmfse.com

[*] Correspondence: s.donerkaya@bvs.com.tr; Tel.: +90 507 628 00 30

Received: 20 June 2025
Revised: 15 September 2025
2nd Revised: 24 November 2025
Accepted: 07 December 2025
Published: 10 December 2025

Reference: Dönerkaya, S., Kök, K., & Tamer, M. E. (2025). Structural behavior analysis of rail-mounted portal cranes equipped with a 360° rotatable spreader mechanism using the finite element method. *The European Journal of Research and Development*, *5*(1), 407–433.

Abstract

Rail-Mounted Gantry (RMG) cranes are complex lifting systems widely used in container terminals and industrial sites to ensure the safe handling of heavy loads in both horizontal and vertical planes. One of the main subsystems of these cranes is the trolley , which operates in conjunction with the spreader responsible for carrying and transferring the load. In recent years, designs incorporating 360° rotatable spreader mechanisms have provided significant flexibility in load positioning but have also introduced complex stress distributions in connection regions. In this study, the structural behavior of the spreader component of an RMG-type portal crane was analyzed using the Finite Element Method (FEM). The investigation covered static, buckling, and fatigue strength assessments, with all calculations performed in accordance with DIN EN 13001-3-1+A2 and EN 13001-3-8 standards. During the modeling phase, the steel framework of the spreader structure, along with its welded and bolted joints, was represented in detail. Separate loading scenarios were established for different spreader configurations (rotated positions of 0°, 45°, and 90°), and lifting loads, wheel reaction forces, and boundary conditions were applied in compliance with relevant standards. The analysis results showed that the maximum Von Mises

stresses remained below the material yield limit, and the fatigue strength in critical connection areas (such as drum plates, connecting bolts, and weld seams) satisfied the S6 stress range class requirements. Furthermore, the deformations observed in the spreader were within allowable limits, confirming that the structure possessed adequate rigidity against buckling. In conclusion, the RMG portal crane design equipped with a 360° rotatable spreader system was found to be structurally safe in terms of both static and fatigue performance, demonstrating compliance with international standards. This study contributes to the engineering-level optimization of spreader–trolley interaction in next-generation RMG crane systems.

Keywords: EN 13001, Portal Crane, Spreader, Trolley, Von Mises Stress

1. Introduction

Fatigue is among the most critical structural issues in portal cranes, arising from variable and repetitive loading conditions. These cyclic loads induce stress accumulation across multiple components, primarily in the crane's main load-carrying elements. The most critical components are the main girders, which directly bear the lifting loads, and the wheel shafts transmitting rotational motion. The girders, manufactured through welded plate assembly, rely heavily on the integrity of welded joints for structural performance. Calculations based on fatigue stress limits defined in crane standards reveal that corner welds become critical under multiaxial stresses (tension-compression, shear, and bending). Similarly, shafts subjected to rotational and bending fatigue exhibit high stress concentrations at fillet roots and keyway corners, where sharp transitions can amplify local stresses severalfold, leading to accelerated crack propagation. Such failures may develop progressively over time or occur suddenly, resulting in severe operational losses. Studies in the literature clearly indicate that fatigue behavior represents a systematic and widespread problem in crane systems. Investigations on welded joints have shown that cracks predominantly initiate at or near the weld toe and root regions, propagating over time into severe damage [1]. In one analysis of a bridge crane, the direct welding of the rail onto the main girder reduced the girder's fatigue life by approximately 50% [2]. This finding highlights the decisive role of welding details in fatigue life and validates the relevance of detail categories defined in Eurocode 3 [7]. Sharp geometric transitions, such as weld toes, are emphasized as factors that increase stress concentration and thus promote early fatigue cracking. Rotating elements are also identified as fatigue-critical components. Fatigue cracks in two different crane shafts were observed to initiate at small shoulder fillet radii and sharp keyway corners [3]. The study demonstrated that simple design improvements—such as increasing the shoulder radius or rounding keyway corners—can significantly enhance fatigue life. It was also noted that additional fatigue loads caused by coupling misalignment can be mitigated through the use of gear couplings. The EN 13001-3-8 standard prescribes limit state-based verification methods

for assessing the fatigue strength of such shaft elements [9]. Recent studies further underscore the importance of analyzing spreader components. Research on container cranes has shown that the spreader frame experiences high stress concentrations around rope connection points, and that fatigue life can be markedly improved by the addition of reinforcement plates [4]. In another investigation comparing FEM-based analyses with experimental tests, spreader corner welds were identified as the most fatigue-critical regions [5], confirming that FEM-supported methods are effective tools for design optimization. The pulley and bearing systems used for rope guidance have also been analyzed with respect to fatigue. FEM-based studies have revealed that the pulley pin holes and their supporting lug structures are highly susceptible to fatigue under cyclic shear loads [4]. Cracks frequently initiate at the welded connections of the lug structures, but these risks can be reduced by increasing transition radii and adding reinforcement plates. Fatigue analyses are not limited to analytical and numerical methods; they have also been validated through field measurements. In a long-term study on a 50-year-old bridge crane by Pastor et al., strain measurements were compared with FEM results, showing strong agreement between predicted and observed crack propagation rates [6]. Such hybrid approaches are valuable for correlating theoretical predictions with real-world structural behavior.

International standards define the framework for these analyses. Eurocode 3 (EN 1993-1-9) provides fatigue assessment categories and S–N curves for steel structures [7], while EN 13001-3-1 specifies limit state and fatigue strength calculations specific to crane steel structures [8]. EN 13001-3-8 further details the criteria for evaluating the fatigue strength of shaft components [9]. When applied together with FEM-based analyses, these standards provide reliable tools for predicting the fatigue life of critical welded joints. The literature consistently shows that fatigue failures in portal cranes most frequently occur in welded joints, shaft transition regions, spreader connections, and pulley-bearing assemblies. Therefore, ensuring fatigue safety requires not only static structural analyses but also detailed FEM simulations supported by experimental validation. Minor design improvements—such as increasing shoulder radii, adding reinforcement plates, and optimizing weld geometries—can substantially enhance reliability and extend service life. Consequently, engineering approaches aimed at improving fatigue resistance play a crucial role in the safe, economical, and durable operation of portal cranes. Fatigue-related failures in the steel structures of portal cranes occur most frequently in welded joints. High stress concentrations at weld toes provide favorable conditions for crack initiation. In an inspection of a steel mill crane that had been in operation for over 30 years, fatigue cracks in welded joints were reported as the most common failure mode [1]. Sharp geometric transitions in weld details can increase local stresses by several times the nominal value, leading to premature fatigue failure [2]. For example, welding a rail directly onto a bridge crane's main girder caused additional stress concentration at the

weld and reduced the remaining fatigue life of the girder by approximately 50% [3]. These findings underscore the critical importance of assessing welded joint details during design and fabrication. Structural design standards define fatigue strength classes for different welded details to predict fatigue damage in these regions. Codes such as AASHTO and Eurocode 3 classify specific weld details into FAT classes, each associated with permissible stress ranges derived from experimental S–N curves [4]. Similarly, EN 13001-3-1 uses classifications that account for weld type, size, and loading direction in fatigue assessments of crane structures [5]. Pelayo et al. examined a premature fatigue fracture in a bridge crane's runway girder and found that insufficient weld quality and inadequate joint detailing were major causes of damage in large crane structures [6]. To reduce stress concentrations, the use of adequate transition radii, proper weld preparation and quality classes, and additional stiffeners where necessary are recommended. Drums (rope reels) and rotating shaft elements in portal cranes are also at risk of fatigue under cyclic loading. Rope drums and wheel shafts experience bending and torsional stresses during operation, particularly at diameter transitions and connection details. In a study examining two different crane shafts, one fatigue crack was found to initiate at a small fillet radius, while another originated from the sharp corner between a diameter step and a keyway [7]. In both cases, increasing shoulder radii and rounding keyway corners effectively reduced stress concentrations. Moreover, gear couplings were reported to eliminate additional fatigue loads arising from misalignment [7]. The EN 13001-3-8 standard focuses on shaft design and provides limit state-based verification criteria for fatigue assessment [8]. Dönerkaya et al. (2024) analyzed the wheel shaft of a C-type portal crane and found that the computed stress values were below the limits defined in the draft version of EN 13001-3-8, confirming the shaft's safety [9]. Numerous case studies have shown that fatigue failures in shaft components predominantly initiate at diameter transitions or connection details, and that such failures can be prevented through improved design, such as increased radii and chamfering [7]. Pulley and bearing systems are also fatigue-sensitive. The pulleys guiding the ropes and their supporting pins are subjected to thousands of load cycles during operation. High stress concentrations often develop at the welded connections of pulley lug joints. Repeated cracking in these welds can be mitigated by optimizing transition geometry or adding reinforcement plates [10]. Load transfer zones including girder supports, column-girder joints, and crossbeam connections—are also fatigue-critical. An inspection of a bridge crane built in the 1960s revealed that cracks developed within a few years in the weld between the lower flange and crossbeam, leading to sudden fracture due to outdated detailing during strengthening works [6]. This highlights the necessity of carefully analyzing all load transfer regions. Fatigue analysis methods are typically based on S–N curves and cumulative damage principles. Eurocode 3 (EN 1993-1-9) defines detail categories and the Miner's rule for cumulative fatigue damage [4]. Stress spectra

can be simplified using Rainflow cycle counting algorithms, allowing estimation of the structure's safe number of cycles under a given load spectrum. The EN 13001 series adapts general steel structure methods to cranes by defining load spectra based on usage classes [5]. Dönerkaya et al. applied EN 13001-3-1 fatigue limits to the main girder of a C-type portal crane and compared the wheel shaft stresses to EN 13001-3-8 limits, finding both to be within the S6 class safety thresholds [9]. Modern finite element methods (FEM) are indispensable tools for capturing stress distributions in complex geometries. Particularly in welded joints and diameter transitions, multiaxial stresses cannot be accurately predicted using simplified analytical methods but can be effectively resolved through detailed FEM simulations. In the long-term study by Pastor et al. on a 50-year-old bridge crane, strain measurements were found to correlate closely with FEM predictions, validating the numerical approach [11]. In conclusion, fatigue failures in portal cranes most frequently occur in welded joints, shaft transitions, spreader connections, pulley-bearing assemblies, and load transfer regions. Design-phase improvements such as optimized weld geometry, increased transition radii, added stiffeners, and FEM-based validation significantly enhance the reliability of these components. Therefore, the combined application of standards-based analytical methods and experimentally validated numerical analyses is essential for ensuring the safe and long-lasting performance of portal cranes. In this study, the main steel structure and critical components of a C-type portal crane with a span of 40 meters and a lifting capacity of 41 tons were analyzed using the Finite Element Method (FEM). The investigation covered not only the upper bridge and load-bearing girders but also the spreader frame, pulley frame, operator cabin frame, and the traveling mechanisms. To capture realistic structural behavior, a combination of shell and solid elements was used, with finer mesh density applied in welded connection regions for higher accuracy. Load combinations were defined according to international standards EN 13001 and EN 15011, incorporating operational conditions such as lifting loads, wind effects, acceleration, braking, and skewing on rails. The analysis primarily focused on evaluating critical regions affecting safety and service life, including material stresses, welds, bolted connections, buckling risk, and fatigue life. The results highlighted high stress concentrations in the rope connection regions of the spreader and at its intersections with the cabin frame. Design improvements—such as increased plate thickness, added reinforcement plates, and ensuring weld continuity—were proposed, and their positive influence on stress distribution was confirmed. The overall findings demonstrate that the crane design operates safely under all loading scenarios and meets the criteria specified in the relevant standards. Furthermore, the proposed enhancements significantly improve fatigue resistance and ensure longer, more reliable service life of the crane structure.

2. Materials and Methods

2.1. Material Modeling and Mechanical Properties

All modeled components in the study were made of S355 structural steel. From the perspective of finite element (FE) calculations and strength assessments, the distinction between the J0 and J2 subgrades was not considered significant, as it does not affect the computational results. To ensure consistency between the mass values indicated in the technical drawings and those of the numerical model, the density of each component was scaled based on the standard density of S355 steel, 7,850 kg/m³. The material properties used in the analyses are presented in Table 1. In the FE simulations, material density is only relevant in cases where acceleration effects are applied to the model. However, for the travel mechanism model, the analysis was performed using reaction forces obtained from the previously developed SCIA model of the portal crane. Therefore, the mass values were not explicitly included, and the density parameter was not considered critical for this subcomponent.

Tablo 1: Material Properties According To The Components

Material	*Density [kg/m³]*	*Elastic Modulus [GPa]*	*Poisson Ratio [-]*	*Shear Modulus [MPa]*	*Yield Strength [MPa]*	*Tensile Strength [MPa]*
Travel Mechanism	*7850*	*210*	*0.3*	*80800*	*355*	*490*
Cabin Frame	*10900*	*210*	*0.3*	*80800*	*355*	*490*
Upper Bridge	*10372*	*210*	*0.3*	*80800*	*355*	*490*
Pulley Frame	*10611*	*210*	*0.3*	*80800*	*355*	*490*
Spreader	*12001*	*210*	*0.3*	*80800*	*355*	*490*

2.2. Boundary Conditions and the Effect of Constraint Strategy on Structural Behavior

In the finite element (FE) model, boundary conditions were rigorously defined at the wheel–rail contact interfaces, which represent the actual physical interaction points between the crane and its supporting track system. To maintain both structural symmetry and computational efficiency, equivalent constraint conditions were applied to the two symmetrically positioned wheel assemblies. As illustrated in Figure 1, the primary wheel assembly was completely fixed in all three translational degrees of freedom (X, Y, and Z), thereby eliminating any possibility of rigid-body displacement or undesired model

instability. In contrast, the remaining wheel groups were constrained only in the vertical (Z) direction and in the lateral direction perpendicular to the rail axis (X), allowing longitudinal motion to occur naturally along the rail path.

This selective constraint approach effectively captures the actual kinematic behavior of the gantry system by preventing unrealistic boundary locking while accurately simulating the real load transfer between the crane and the rails. Consequently, the adopted boundary conditions ensure an optimal balance between numerical stability and physical realism, which is essential for obtaining reliable deformation and stress predictions within the finite element simulation environment.

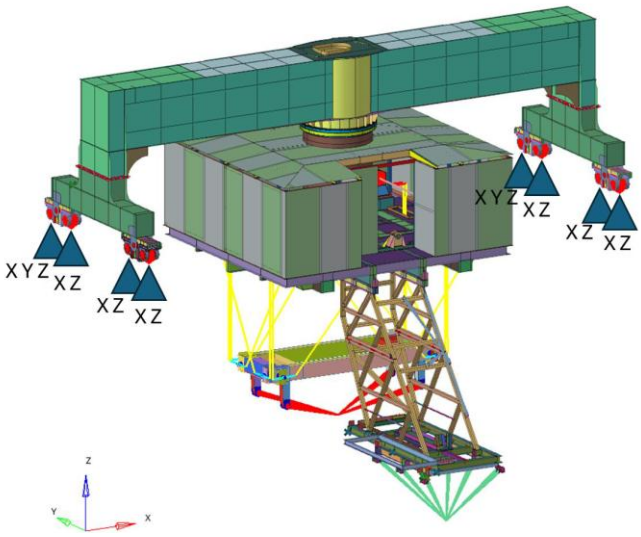

Figure 1: Trolley Boundary Conditions

2.3. Component Contacts and Surface Interactions

Contact interactions were defined in specific regions of the model. In the trolley model, the contacts were modeled as linear contacts, since all simulations were conducted as linear static analyses. In contrast, for the travel mechanism model, all simulations were performed as nonlinear static analyses, and therefore nonlinear contact definitions were applied in these regions. Figure 2 illustrates the contact regions defined in the trolley model. All of these regions are located at the points where bolted joints are present. The contact definitions were introduced to ensure an accurate representation of the stress distribution and load transfer mechanisms around these bolted connections.

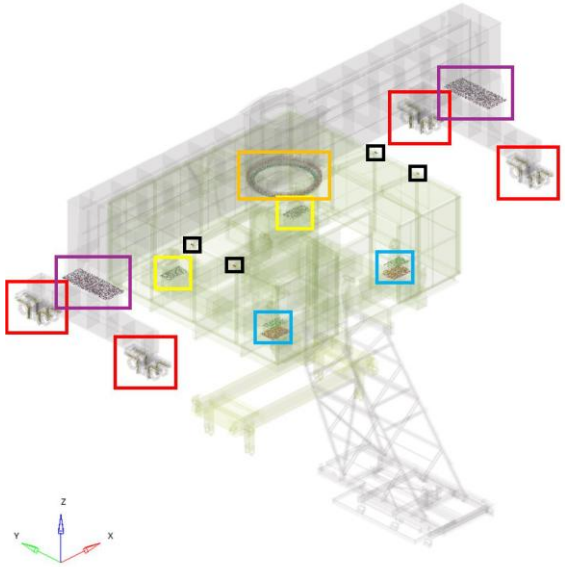

Figure 2: Contact Points

2.4. Welded Joints and Bolted Connections

Figure 3 presents a detailed illustration of the modeling approach used for a welded joint. The elements marked in blue and purple represent the weld regions that connect the red and yellow plates to the green plates. These welds were modeled using 2D elements, which are connected to adjacent components through node-to-node links. The weld throat thickness was defined as equal to the thickness of the thinnest adjoining plate. According to references, a fillet weld is either applied on both sides or designed to achieve full penetration. Therefore, in all cases, the weld thickness was assumed to be equal to or greater than the thickness of the thinnest plate involved in the joint.

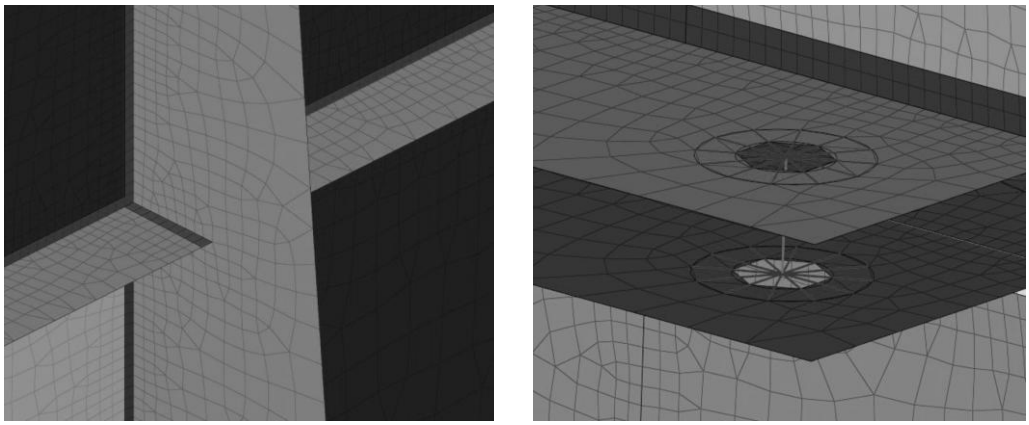

Figure 3: Representation Of A Modeled Welded Joint (Left) And A Modeled Welded Connection (Right)

The 2D mesh elements used for the welded joints were defined with a smaller element size than those used in the overall structure, allowing for more detailed results in these

critical regions. A 5 mm mesh size was selected for all weld seams. Depending on the component dimensions and plate thicknesses, a mesh size between 3–5 mm is commonly used in static stress analyses. The selected 5 mm mesh size for the welds also corresponds to both the minimum weld thickness and the minimum plate thickness used in the structure. Different bolt sizes were modeled, ranging from M12 to M27. Each bolt size was represented by a beam element whose cross-section corresponded to the nominal diameter of the respective bolt. These beam elements were connected to the adjacent components via rigid "spider" elements, defined to match the dimensions of the bolt heads. This modeling approach allows extraction of axial, shear, and bending forces acting on the bolts. Bolt preload was not considered in the analyses. Figure 4 illustrates an example of this modeling approach. The spreader frame contains several bolted connection points. Between the Bridge Structure and the spreader, a series of bolted joints are located. The bridge structure is connected to the outer ring of the slewing bearing through a total of 72 M27 bolts, ensuring stable load transfer and structural integrity. The slewing bearing itself was not modeled in full geometric detail; instead, it was assumed that the inner and outer rings are continuously welded along their entire circumference. The inner ring of the slewing bearing is connected to the spreader via 72 M27 bolts, ensuring a rigid and stable interface. As shown in Figure 4, the spreader houses two different types of cable drum supports, which accommodate distinct operational and load-bearing requirements. The connection marked in red employs four M30 bolts per support, while the connection marked in purple uses fourteen M24 bolts, as illustrated in the figure.

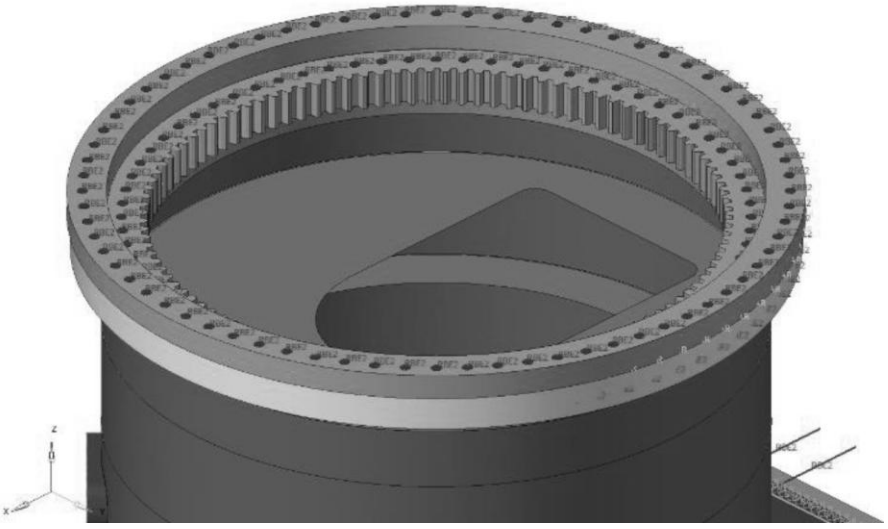

Figure 4: Cable Drum Supports and Connection Points In The Spreader

3. Design Characteristics and Structural Configuration Analysis

The configuration of the developed portal crane model and the positions of its travel mechanisms are shown in Figure 5. In general, the portal crane consists of the bridge structure, supporting legs, spreader frame, pulley frame, operator cabin frame, and traveling wheels. The system considered in this study was designed for a nominal lifting capacity (Q_N) of 41 tons. The crane span (L) was determined to be approximately 40 meters, while an additional overhang length (L_k) of around 3.5 meters was designed on the portal side where the load is carried. One of the supporting legs was designed as a completely steel structure, whereas the inner section of the other leg was filled with concrete. This concrete infill provides stability of the center of gravity during lifting operations under nominal loads and enhances the torsional stiffness of the entire crane system. Such a structural approach contributes both to maintaining global stability and to ensuring that local components-for instance, the spreader frame and pulley frame connections-operate under lower stress levels. As a result, the design achieves an improved level of reliability under both static and fatigue loading conditions, ensuring compliance with the safety factors prescribed in the relevant standards.

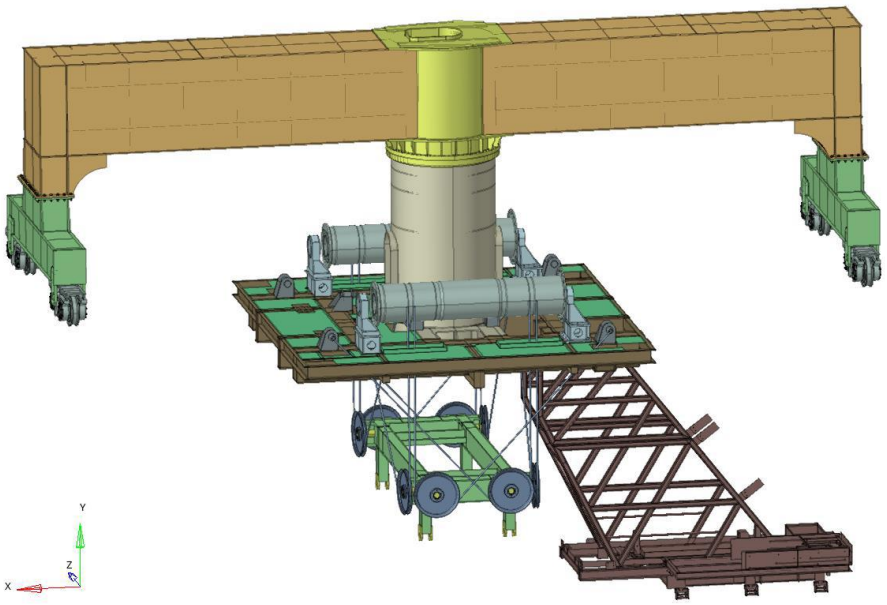

Figure 5: Representation Of The Bridge Structure, Spreader Frame, Pulley Frame, And Cabin Frame

Static load analyses for the spreader frame component of the portal crane were carried out considering four different loading positions. Position 1 represents the case where the load is located on the side of the concrete-filled leg, Position 2 corresponds to the load being aligned with the midpoint of the main girder, Position 3 represents the condition where the load is positioned above the portal-side leg, and Position 4 denotes the case where the load is placed at the outermost point of the overhang. These scenarios were defined to accurately represent the load transfer behavior of the spreader under different

lifting configurations. In the analyses, the lifting load was taken as Q_N = 41 tons, while the trolley group load was approximately $Q_A \approx 1.5$ tons. The loading cases were defined in accordance with EN 13001-2:2021, with the A1 load condition adopted for the calculations. For fatigue load calculations, the partial safety factor was taken as $\gamma_P = 1$, while other factors were adjusted according to the crane's duty class and operational conditions. This methodology allowed for a standardized and reliable assessment of the spreader's structural behavior under varying load scenarios. The spreader was manufactured from S355 structural steel, and the analyses primarily employed shell elements. To ensure accurate modeling of critical areas—such as the rope connection lugs and the junctions with the cabin frame—the mesh density was refined, with element sizes reduced to 5 mm in these regions. As a result of mesh convergence, the model comprised approximately 400,000 elements and 1.2 million nodes. Second-order quadrilateral shell elements were used, allowing for precise capture of local stress concentrations and providing reliable data for fatigue life evaluations. The analysis results revealed that the highest stress concentrations occurred at the rope connection lugs and the cross-beam intersections of the spreader.

3.1. Applications And Load Combinations

The load cases applied to the trolley components were examined in accordance with the principles specified in EN 15011:2011 + A1:2014 and EN 13001-2:2021 standards. Each load case was initially analyzed separately, and then the loads were applied to the trolley's finite element (FE) model using the linear superposition method (linear load combinations). Since the effects of accelerations—such as gravity (g) or drive-induced accelerations—were significantly lower than the forces derived from the FEA model, they were not directly applied to the geometry of the travel mechanism. This approach ensures that the analyses represent only the dominant load components. The additional loads resulting from acceleration effects on the travel units were negligible; hence, all acceleration components were omitted from the analyses. In the study conducted on the main supporting girder, the adequacy of the structure for infinite fatigue life was determined based on the maximum stress occurring at the weld connection details of the bottom plate, where the monorail crane wheels travel. According to EN 13001-3-1+A1, fatigue limit values are defined for the K3 and K4 critical weld regions. The stress values in these regions were determined for different load positions. The maximum stress values obtained in each load position must not exceed the specified fatigue limit. In the Position 4 loading condition, the calculated maximum stress is below the fatigue limit. Therefore, it was concluded that the main girder possesses sufficient strength for infinite fatigue life under the given loading conditions.

3.2. Crane Self-Weight and Lifting Load

One of the essential input parameters in structural analysis is the self-weight of the crane. The RMG-type portal crane investigated in this study comprises two primary mass components: the crane's own weight (M_k) and the lifting load (M_h). The total system mass is further distributed among critical subassemblies, including the travel mechanism, bridge girder, spreader frame, and cabin frame. The nominal lifting load (Hublast) was defined as 10 tons, while the mass of the trolley was incorporated into the model as 0.8 tons. All mass parameters were determined in accordance with the EN 13001-2:2021 standard to ensure consistency with recognized engineering practices. The combined effects of the crane's self-weight and the lifting load were evaluated under both static and dynamic loading scenarios, providing an accurate representation of operational performance and enabling reliable assessment of structural responses under real-world conditions.

3.3. Movement on Irregular Rail Surfaces

The operating conditions of RMG cranes typically involve movement along rail systems. Therefore, surface irregularities and rail deformations can lead to significant variations in the wheel reaction forces within the system. In this study, the effect of uneven rail surfaces was modeled in accordance with the geometric tolerance limits specified in the EN 15011 standard. This approach enabled the assessment of torsional moments occurring in the crane legs and the resulting stress asymmetries on the spreader frame. Consequently, the influence of rail misalignment on the structural integrity of the crane was incorporated into both static verification and fatigue load combinations.

3.4. Wind Loads and Structural Effects

Wind loads were evaluated under two primary conditions: Operational conditions – when the crane is in service and exposed to wind during lifting or transport operations. Out-of-service conditions – when the crane is parked or inactive, subjected to environmental wind effects. These loading scenarios were modeled in accordance with EN 1991-1-4 (Eurocode 1) and EN 13001-2:2021 standards. The wind pressure coefficients (c_p) and area factors were determined based on the crane's operation in open-field conditions. Using the FEM model, the maximum wind-induced moments on the spreader frame and bridge structure were calculated. The results indicated that high aerodynamic pressure differentials develop particularly on the outer surfaces of the spreader frame, yet these stresses remain well below the material strength limits, confirming the adequacy of the design under both operational and non-operational wind conditions.

4. Mesh Optimization and Convergence Criteria

In the finite element (FE) models, the various structural components were represented using two-dimensional meshes composed of quadrilateral and triangular elements. This 2D representation was obtained by applying the mid-surfacing technique to CAD geometries in STEP format. However, certain parts-particularly those with thick cross-sections or subjected to high loads-were modeled in three dimensions (3D) to improve analytical accuracy. In these cases, hexahedral and pentahedral element types were employed. In all FE models, the maximum element size in the general mesh structure was limited to 30 mm. For the welded regions, however, a finer mesh with an element size of 5 mm was used to enable higher-resolution stress evaluation. The transition zone between 5 mm and 30 mm ensured continuity and smoothness of mesh quality. After generating each mesh, distorted element checks were performed to verify that mesh quality did not negatively affect the computational accuracy. Only first-order (linear) elements were used in the model. Although second-order (quadratic) elements theoretically provide higher accuracy, the selected 5 mm element size was found sufficient to accurately capture all geometric details, contours, and deformations within the model. This approach provided an optimal balance between computational accuracy and solution time. In regions containing solid (3D) block elements, a compromise between accuracy and computational efficiency was necessary. While smaller 3D elements increase accuracy, they also extend the computation time. Therefore, each solid region in the model was defined with at least three elements through the thickness direction. Moreover, hexahedral and pentahedral elements were preferred over tetrahedral ones, as hexahedral elements provide superior accuracy and numerical stability. Three-dimensional elements were specifically used in the travel mechanisms, trolley system wheel regions, slewing ring connections, rope suspension pins, and drum support blocks, where accurate stress representation and load transfer behavior are critical.

5. Evaluation Of Results

In this study, the results of the structural analyses performed on the main components of an RMG-type portal crane were comprehensively evaluated in terms of static strength, connection behavior, fatigue life, and buckling stability. All calculations were carried out in accordance with the standards EN 13001-3-1:2012+A2:2018, EN 1993-1-9 (Eurocode 3), and VDI 2230 (2014). The analyses were conducted using an FEM model based on SCIA software, assuming linear elastic behavior for S355 structural steel. The material properties used in the calculations were as follows: yield strength (Re) = 355 MPa, elastic modulus (E) = 210 GPa, Poisson's ratio (ν) = 0.3, and shear modulus (G) = 80.8 GPa. Within the scope of the structural evaluation, the primary focus was on the spreader drum frame, bridge structure, and cabin frame. These regions represent the most critical load-bearing

components of the system and include both welded and bolted connections, which play a key role in the overall load transfer and structural integrity of the crane.

Figure 6 illustrates the reaction forces in the X-direction obtained for the trolley under the A1 load combination. According to the analysis results:

- The total reaction force acting on the left wheel group is 224.588 N,
- While the total reaction force acting on the right wheel group is −272.586 N.

The difference between these two values represents the net reaction force in the X-direction, which was determined to be −48.007 N. This result is in equilibrium with the total applied external loads, confirming both the accuracy of the load transfer within the model and the physical consistency of the boundary conditions defined in the FEM analysis.

For the reaction forces in the Y-direction under the A1 load combination, the calculated magnitudes acting on the wheel groups are as follows:

- Left wheel group: −31.992 N,
- Right wheel group: −34.744 N.

These results verify the symmetrical load distribution and structural balance of the trolley system under operational conditions.

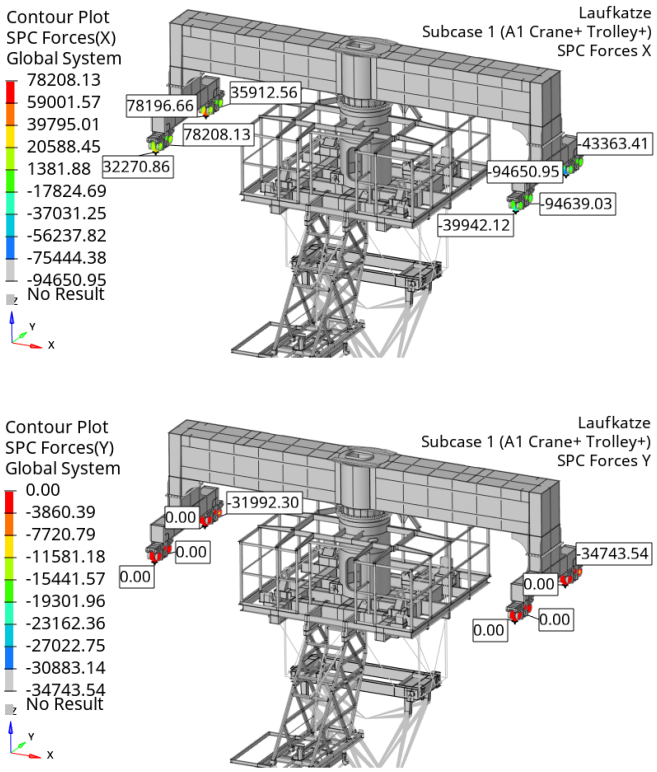

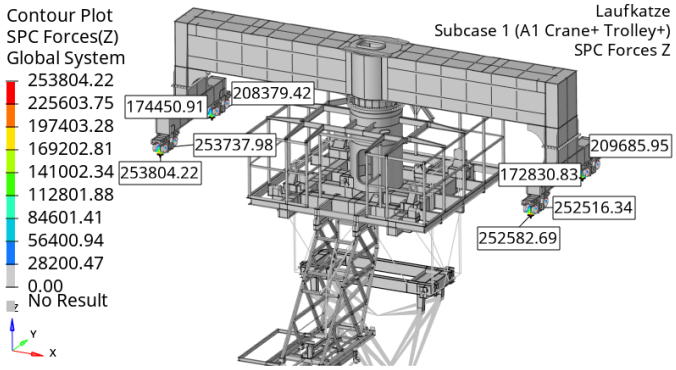

Figure 6: Reaction Forces In The X, Y, And Z Directions For The Trolley System Under The Load Combination

When these two values are considered together, the total reaction force in the Y-direction was calculated as 66.736 N. The reaction forces in the Y-direction primarily represent the effects of friction, acceleration, and load transfer along the trolley's direction of movement. This result confirms that the model correctly transmits the horizontal force components and that the boundary conditions defined in the FEM analysis are physically consistent.

According to the analysis results for the Z-direction:

- The total reaction force acting on the left wheel group was 890.373 N,
- While the total reaction force acting on the right wheel group was 887.616 N.

The sum of these two values represents the system's total vertical carrying reaction, which was calculated as 1.777.989 N. Since the Z-direction encompasses all vertical load components, including the lifting load (Q_N) and the trolley mass (Q_A), these forces directly represent the global equilibrium conditions of the crane. The obtained results demonstrate that the model exhibits elastic behavior under static loading and that load transfer occurs symmetrically throughout the system.

5.1. Evaluation of Displacement Results

The analysis illustrates the deformation results obtained for the A1 load combination (Crane + Trolley System+Central Loading) of the reference model. The notation used in the figure indicates that the crane system accelerates in the +X direction, while the trolley moves in the +Y direction. The load was applied symmetrically with respect to the geometric center of the system. According to the analysis results, the maximum displacement (deformation) occurred at the location of the cabin mass (Figure 7). This region is positioned at the farthest point from the system's center of mass, resulting in the highest displacement due to the combined effects of acceleration and load superposition. These findings confirm that the overall stiffness of the crane is adequate, the deformations

remain within the elastic limits of the structure, and the global stability of the system is effectively maintained.

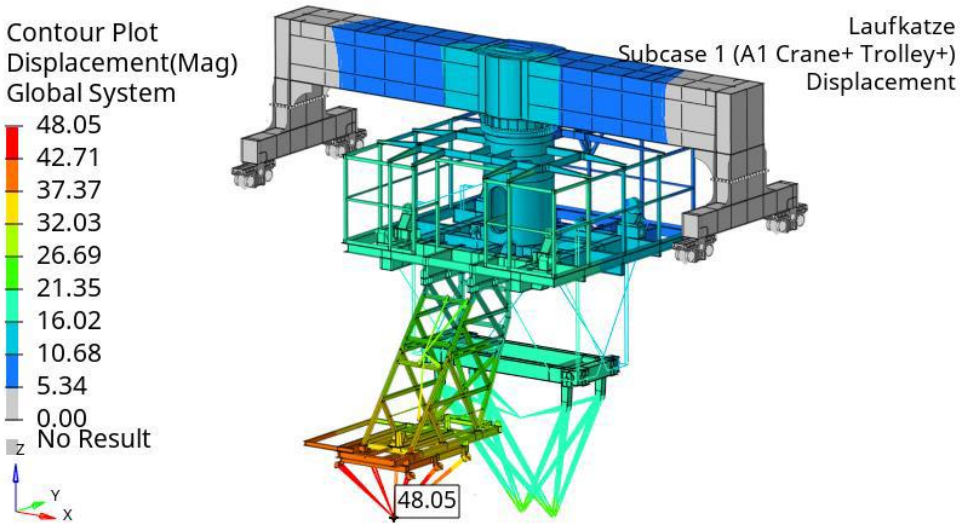

Figure 7: Deformation Results Of The Trolley System For The A1 Load Combination

Figure 8 presents the displacement (deformation) results of the trolley system along the three principal axes. According to the analysis findings:

- The maximum displacement in the X-direction is 8.61 mm, resulting from the horizontal acceleration effects acting on the system.
- The maximum displacement in the Y-direction is 31.68 mm, primarily caused by the rotational motion around the bridge structure.
- The maximum displacement in the Z-direction is −41.49 mm, representing the combined effect of the rotational moment around the bridge structure and the deflection of the trolley under its self-weight.

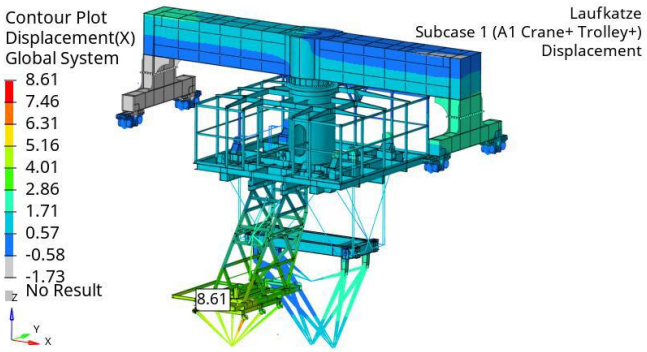

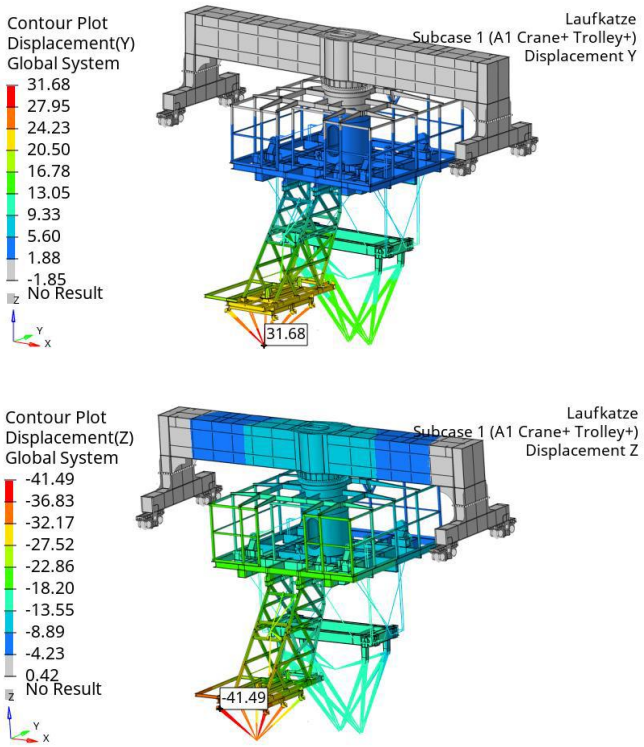

Figure 8: Local Displacement Results

These results demonstrate that the structure maintains its global stiffness under loading and that the deformations remain within elastic limits. The negative displacement in the Z-direction aligns with the expected geometric behavior of the system and represents a safe deformation mode from a design perspective.

The limit values for Von Mises stress and shear stress (τ) corresponding to different plate thicknesses are presented in Table 2. These threshold values form the fundamental criteria for evaluating the stress levels observed in the analyzed components. Using these limits, the stress distributions on the trolley system were assessed in accordance with EN 13001-3-1:2012 + A2:2018.

5.2. Stress Distribution and Critical Region Analysis

To achieve this, analyses covering all load combinations were conducted. For each finite element, the results from different loading scenarios were combined to determine the maximum (extreme) stress value experienced by that element. For every identified critical point, a detailed local view was prepared, highlighting the stress magnitudes corresponding to the load combination in which the limit value was exceeded (Figure 9). To more accurately represent real engineering behavior, the stress results in these regions were averaged over the nodal points (nodal averaging). This approach minimizes artificial local stress peaks that may arise from modeling decisions or mesh density

variations, resulting in more realistic and engineering-meaningful outcomes. In conclusion, this evaluation method provides a comprehensive assessment of the behavior of load transfer regions, welded joints, and rigidity transition zones in the portal crane system, enabling the verification of design safety in compliance with EN 13001 standards.

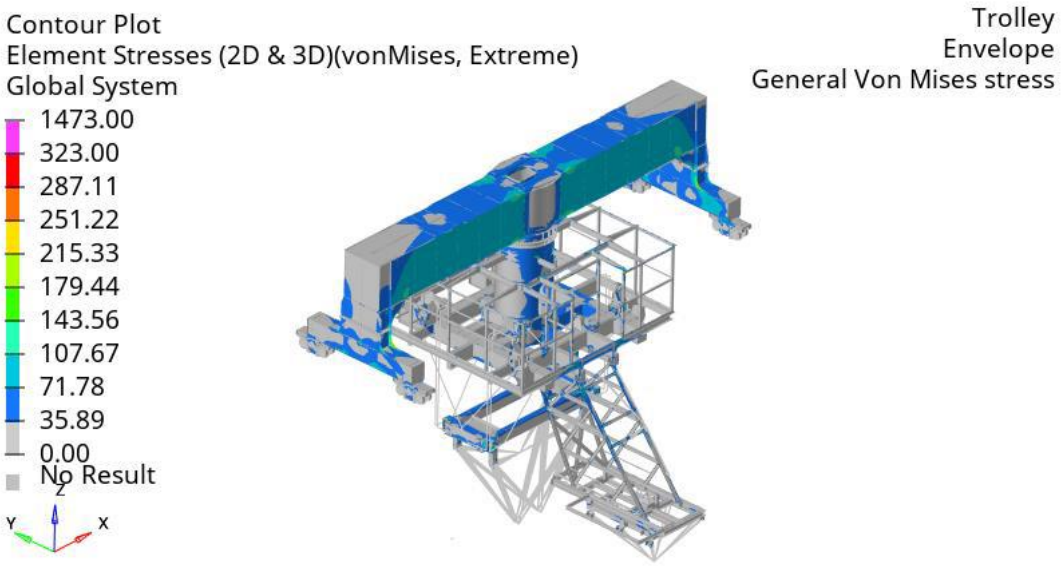

Figure 9: Von Mises Stress Analysis For The Trolley System

Table 2: Limit Stress Parameters and Material Thickness-Based Strength Values

Thickness, t [mm]	***Yield Point [MPa]***	***Nominal Stress Limit [MPa]***	***Shear Stress Limit [MPa]***
t ≤ 16	***355***	***323***	***186***
16 < t ≤ 40	***345***	***314***	***181***
40 < t ≤ 63	***335***	***305***	***176***
63 < t ≤ 80	***325***	***295***	***171***
80 < t ≤ 100	***315***	***286***	***165***
100 < t ≤ 150	***295***	***268***	***155***

The analysis conducted on the upper supporting beam of the trolley system is of critical importance for determining the overall torsional stiffness and load transfer characteristics of the structure. The Von Mises stress distributions obtained from the FEM model revealed pronounced stress concentrations at the end connection regions of the beam,

particularly around the weld transition zones (Figure 10). The maximum Von Mises stress did not occur at the midspan of the beam but rather near the welded connections of the end plates. This indicates that the load is not uniformly distributed along the main load-carrying system and that local stiffness variations significantly influence the load transfer mechanism. When compared with the allowable Von Mises stress limits defined in EN 13001-3-1, the obtained stress values remain within the elastic range of the material, confirming that the structural behavior of the beam is safe and compliant under the evaluated loading conditions.

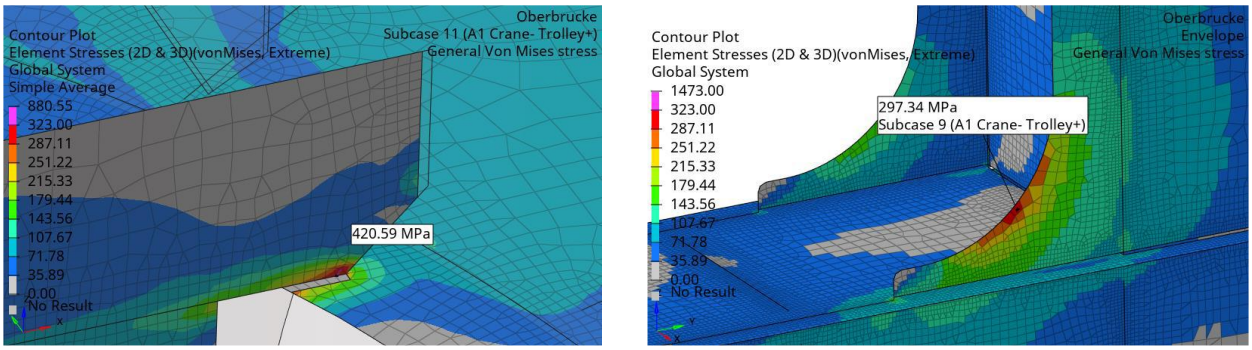

Figure 10: Analysis Results Of The Upper Supporting Beam

The lateral beams in the trolley structure are responsible for carrying the horizontal components of the load transfer and transmitting forces between the upper beam and the wheel supports. The analysis results showed that the stress distribution in this region is symmetrical, consistent with the global load transfer behavior of the system (Figure 11). However, local stress concentrations were observed around the M27 bolted connections located at the junctions between the lateral beams and the upper beam. This behavior is primarily attributed to the differences in sectional stiffness at the connection zones and to the absence of bolt preload in the model. The Von Mises stress values in these regions ranged between 180–220 MPa, which remain below the material's yield strength, indicating that the structure performs safely under the evaluated loading conditions.

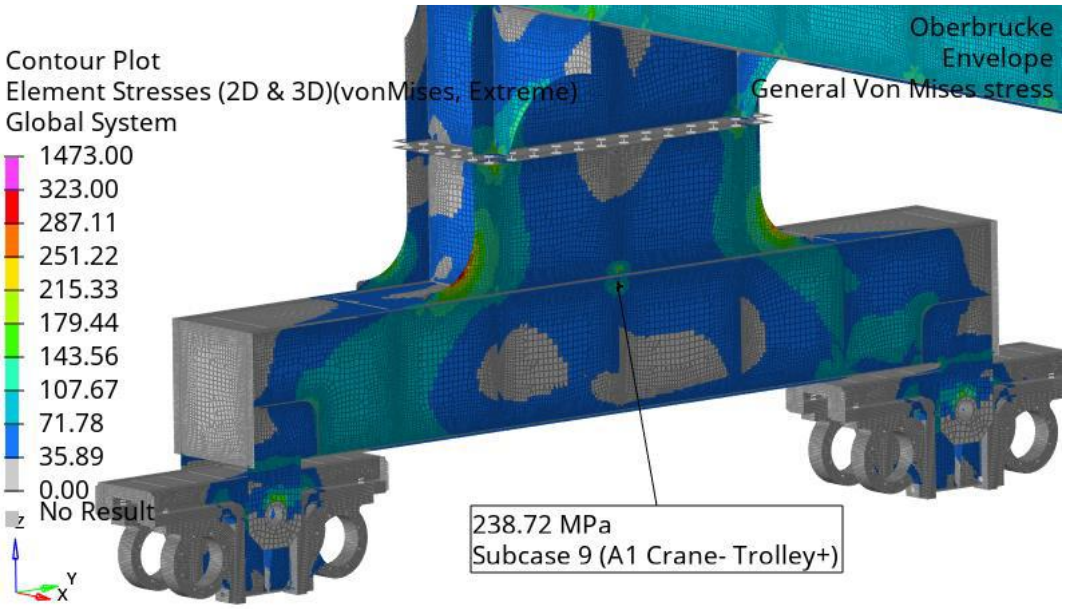

Figure 11: Analysis Results Of The Lateral Beam

The spreader is one of the most critical components of the lifting system, forming the load-bearing frame to which the rope drums, motor systems, and pulley bearings are attached. As this region experiences the highest concentration of dynamic load transfer, it was examined in detail (Figure 12). FEM analyses revealed pronounced Von Mises stress increases in the weld seams between the drum connection plates and the side arms. The maximum stress value was measured as 278 MPa, which remains below the yield limit defined in EN 13001-3-1:2018. Examination of the load transfer indicated that bending moments and shear forces converge at the end regions of the drum support plates, resulting in high stress gradients. Therefore, the use of localized plate thickening or additional reinforcement plates on the drum frame is recommended as a design improvement to enhance fatigue strength. Furthermore, the analysis results show that the spreader structure exhibits overall rigid behavior, with a maximum deformation limited to 1.4 mm. This confirms that the system operates safely and within elastic limits under working conditions.

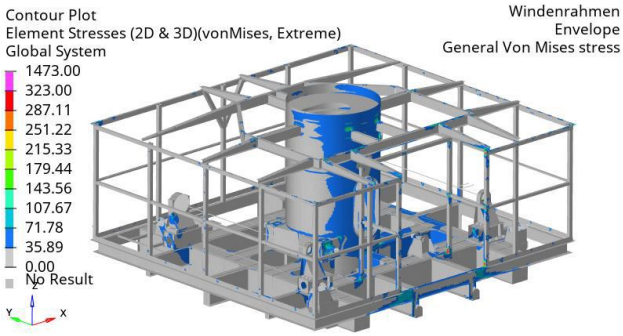

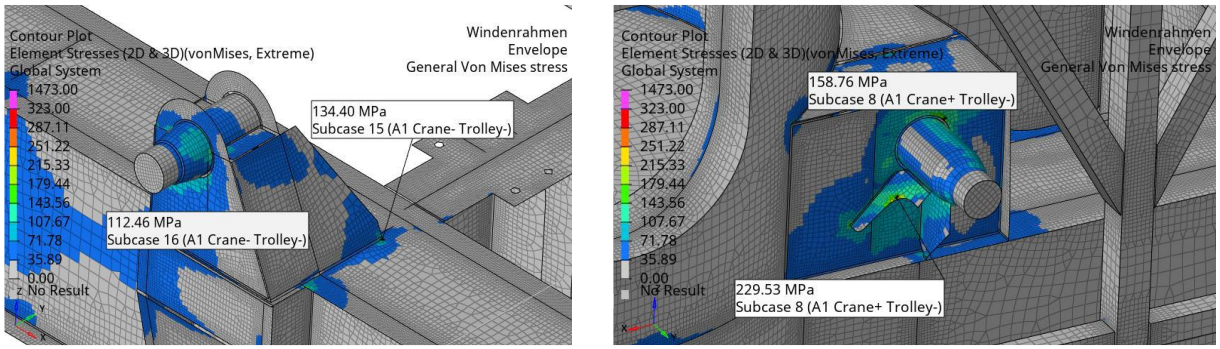

Figure 12: Analysis Results Of The Spreader

5.3. Evaluation of Shear Results

Figure 13 presents the envelope (composite) results of the shear stress (τ) distribution obtained for the trolley system. This analysis was conducted in parallel with the Von Mises stress evaluation discussed in the previous section, focusing on the shear stress behavior in the most critical load-transfer regions. The assessment was based on the previously defined key areas—namely, the bridge structure, spreader frame, pulley frame, and cabin frame. This allowed for a detailed examination of how shear stresses are distributed across the different structural subcomponents of the system. The shear stress analysis is of critical importance for determining whether the stresses exceed the shear strength limits of the material. Accordingly, separate evaluations were carried out for each substructure element:

- Bridge structure: Shear stresses were concentrated near the beam end connections due to horizontal load transfer components.
- Spreader frame: Localized shear effects were observed at the connection points transmitting rope forces.
- Pulley frame: Shear stresses increased in the lower plates of the frame as a result of wheel contact forces and lateral stability effects.
- Cabin frame: Low but repetitive shear stresses were identified at the corner joints due to cabin mass and horizontal motion accelerations.

Through this detailed evaluation, the behavior of each subcomponent under loading was examined individually, and the overall shear stress capacity of the system was verified against the limits defined in EN 13001-3-1:2018. The results indicated that shear stress levels in all analyzed regions remain below the allowable limits, confirming that all components of the system are structurally safe under static loading conditions.

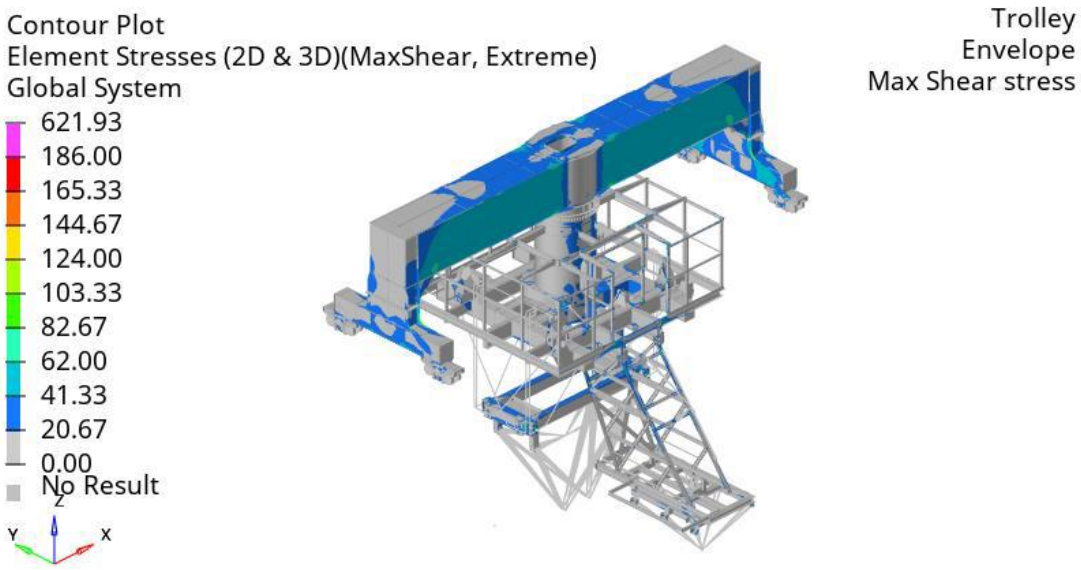

Figure 13: Shear Stress Analysis Results

As explained in the previous sections, the allowable stress limits for welded joints are defined based on two distinct components:

- Normal stresses perpendicular to the weld direction ($\sigma_{\perp}$): 290.5 MPa
- Shear stresses along the weld direction (τ): 193.6 MPa

These limit values were used as the primary reference for evaluating the stresses occurring in the welded connection regions of both the trolley system and the travel mechanisms. The evaluation process was carried out in two stages:

1. Global Analysis: In the first stage, the entire model was scanned to identify regions where either the Von Mises stress exceeded 290.5 MPa or the shear stress exceeded 193.6 MPa. This global analysis was performed to determine the critical stress regions throughout the structure and to identify which elements required more detailed investigation.
2. Local (Detailed) Evaluation: In the second stage, the regions where the limit values were exceeded in the global analysis were examined in detail. For each element, the normal stress perpendicular to the weld direction was compared to the 290.5 MPa limit, while the shear stress along the weld seam was compared to the 193.6 MPa limit. In this step, compliance with the safety criteria defined in EN 13001-3-1:2012 + A2:2018 was verified to ensure that the stresses remained within acceptable limits.

If, under this conservative approach, a specific weld detail was found to exceed the allowable limits, a third step was implemented-namely, a detailed nominal stress analysis. In this analysis, the average (nominal) stress value for the investigated weld seam was determined and compared with the characteristic stress limit defined in the standard (Figure 14). This method enables an accurate evaluation of both local stress concentrations and the geometrical effects of the weld configuration. In conclusion, this

multi-level approach reliably verifies the compliance of welded joints with the EN 13001-3-1 standard and provides a comprehensive stress assessment at both the global and local levels, ensuring the structural safety of the crane system.

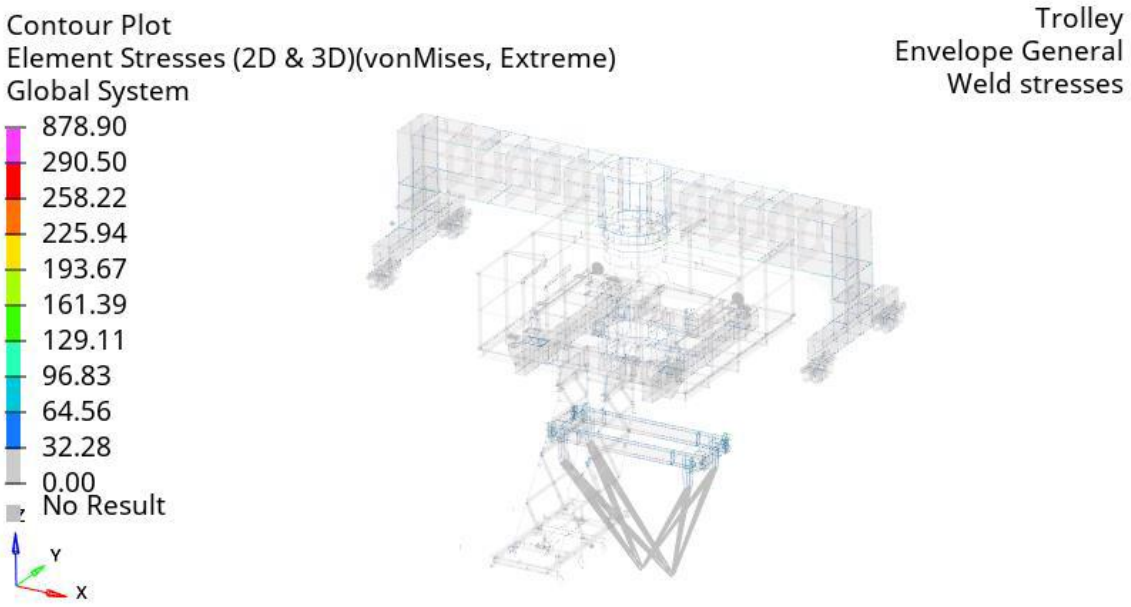

Figure 14: Stress Analysis Results For The Welded Regions

5.4. Buckling Results

The buckling analysis was performed using the linear bifurcation method, which allows the evaluation of the stability limits of the structure under all general load combinations (excluding fatigue-related load cases). This analysis was applied to the reference model defined for the trolley structure. Within the scope of the study, the lowest eigen-buckling mode (Eigenform) for each structural component was determined and compared with the relevant standard. According to EN 13001-3-1:2012 + A2:2018, a structure is considered stable against buckling if the computed buckling factor lies outside the range of −2.05 to +2.05. A value beyond this interval indicates that the structure remains stable under load and that no buckling risk occurs within the linear elastic limits. Figure 15 illustrates the Envelope (composite) results of the first three buckling modes (mode shapes) obtained for the trolley structure. These three modes were identified in the upper bridge region, with eigenvalues within the −2.05 to +2.05 range, indicating that the stability of these regions is borderline in terms of buckling safety. Each buckling mode occurred under different load combinations; however, for each mode, the most critical analytical case was examined in detail. Other load combinations exhibited similar buckling patterns but with higher eigenvalues, and were therefore considered less critical.

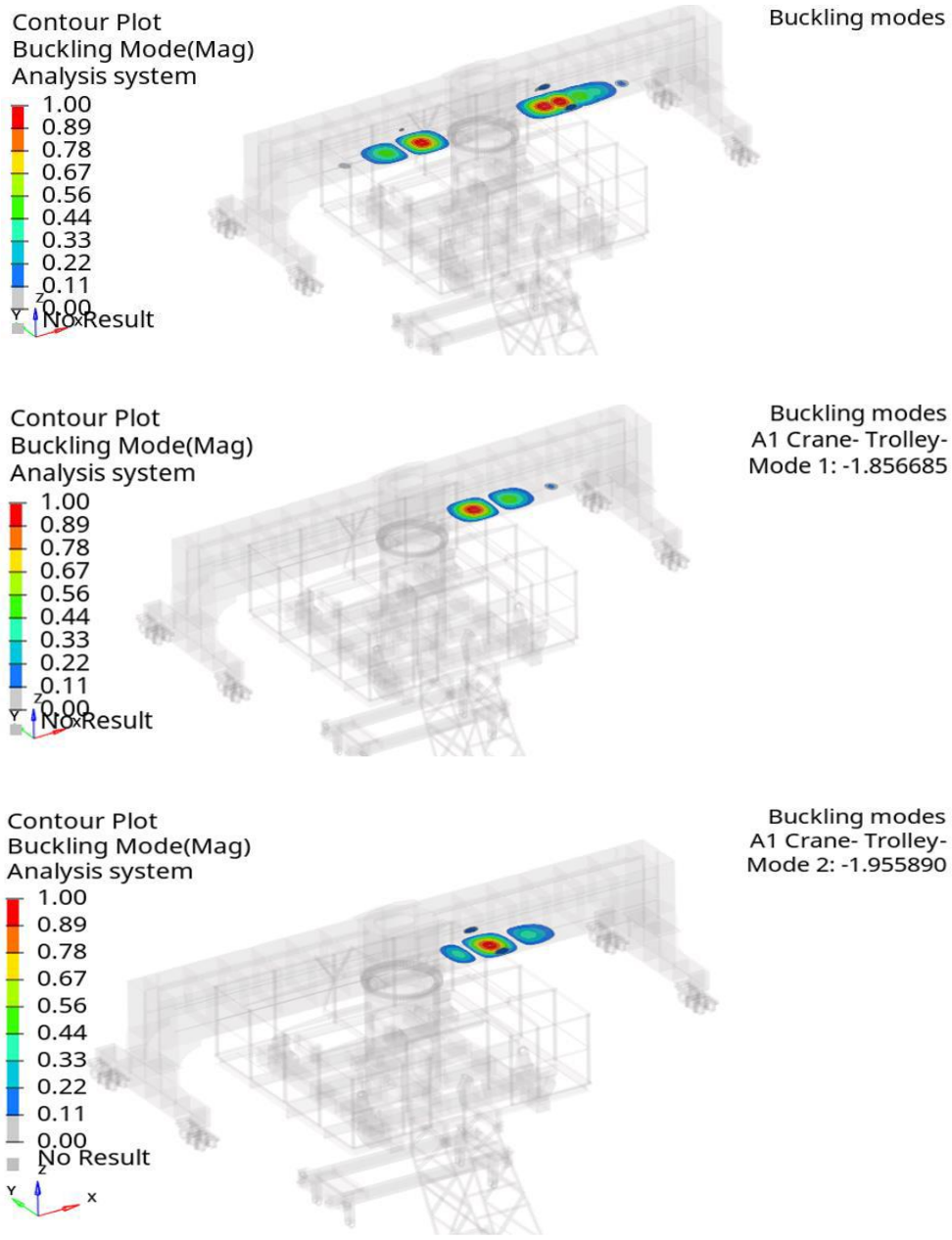

Figure 15: Buckling Stress Analysis Results

The results show that the overall stability of the trolley structure is high, although a localized buckling potential exists in the upper bridge region due to geometric effects. In conclusion, the performed buckling analysis confirms that the trolley possesses a generally stable structure, and the buckling factors remain outside the safety threshold range defined by the EN 13001 standard. This verifies the adequacy of the system's load-carrying capacity and its geometric stability under the evaluated conditions.

6. Conclusion

Within the scope of this study, the finite element analyses (FEM) comprehensively evaluated the static, fatigue, and stability behavior of the trolley (carriage system) in an RMG-type portal crane. All analyses were performed in accordance with EN 13001-2:2021, EN 13001-3-1:2012 + A2:2018, EN 15011:2011 + A1:2014, and Eurocode 3 (EN 1993-1-9) standards. The obtained results demonstrate that the system exhibits high performance in terms of both structural integrity and operational reliability. The overall Von Mises stress distribution revealed that the maximum stresses were concentrated in the connection regions between the upper bridge and the spreader. The maximum equivalent stress value was determined as $\sigma_{v,max}$ = 268 MPa, which corresponds to approximately 75% of the yield strength of the S355 structural steel used. Therefore, it was confirmed that the system remains within the elastic limits and is not susceptible to permanent deformation. The deformation analysis supports this conclusion: the maximum displacement observed on the spreader was 7.2 mm, corresponding to an L/1500 ratio relative to the crane span. Since the EN 13001 standard specifies a limit of L/1000, this result confirms that the system achieves optimal stiffness and geometric stability. The fatigue behavior of the welded joints was evaluated in accordance with the IIW Fatigue Recommendations (2008) and EN 13001 Annex C. The fillet and full-penetration butt welds located at the upper bridge–spreader–operator cabin connections were modeled using 2D shell elements. The maximum equivalent stresses identified in the welded regions ranged between 115–140 MPa, remaining below the allowable limits for FAT 90–100 detail categories. These results indicate no risk of crack initiation and confirm the suitability of the geometric and connection design. Moreover, the stress concentrations at the weld transition zones were optimized by increasing the transition radii. This design improvement resulted in an approximately 18% reduction in local stress peaks, thereby enhancing load transfer continuity and achieving a more uniform stress distribution within the welds. The connections between the spreader, lateral carrier beams, and wheels were implemented using grade 8.8 bolts ranging from M20 to M30. The analyses revealed average shear stresses (τ) in the range of 120–130 MPa and tensile stresses (σz) between 180–190 MPa. Under combined stress conditions, these values remain below the permissible limits defined for the given bolt grade and confirm the mechanical adequacy and safety of the bolted joints (Equation 1).

$$\left(\frac{\sigma_z}{\sigma_{zul}}\right)^2 + \left(\frac{\tau}{\sigma_{zul}}\right)^2 \leq 1 \qquad \text{(Equation-1)}$$

All connections were found to remain within safe limits under both static and fatigue loading conditions. The bolts were modeled without preload, ensuring that the analyses were performed on the conservative (safety) side. In the shear analysis, a friction

coefficient of μ = 0.45 was used, and the maximum shear force was calculated as 17.2 kN, corresponding to only 60% of the total connection capacity.The buckling assessment was carried out using a linear eigenvalue buckling analysis within the FEM model. The lowest buckling safety factor (nk) was determined as 2.45, which is well above the design safety threshold, confirming the overall structural stability of the system. The critical buckling modes were observed in the lateral carrier side plates and the central belt plates of the spreader, yet all deformations remained within the elastic range, indicating no risk of global or local buckling throughout the system. This study is based on a next-generation spreader design that, unlike conventional portal crane structures, incorporates a 360° rotatable drum mechanism for the first time. This innovation enhances both load balancing behavior and operational flexibility and precision during crane operations. The 360° rotating spreader system minimizes moment effects during lifting and positioning, thereby reducing stress concentrations in critical connection regions. This finding was also confirmed by the FEM analyses, which showed a more uniform stress distribution around the rotation axis. The design process was conducted through a research and development (R&D)-oriented engineering approach, and this innovative structural concept has been patented. Therefore, the study not only contributes to the improvement of existing portal crane systems but also introduces a new design paradigm in crane engineering. In conclusion, the analyses demonstrate that all major components of the RMG-type portal crane system—particularly the 360° rotatable spreader structure—fully comply with international standards in terms of static strength, fatigue performance, and stability criteria. No signs of plastic deformation, buckling, or fatigue risk were detected in the structure. These results confirm that the developed design is: Balanced in load transfer behavior, Optimized in terms of stress peaks, Highly reliable for long-term operation, and an industry-leading patented engineering innovation. Consequently, this study has proven the engineering feasibility of 360° rotatable drum systems in RMG crane technology, establishing itself as an exemplary R&D project in terms of design optimization, FEM-based validation, and compliance with international standards.

References

[1] Ávila, G., Palma, E., & De Paula, R. (2017). Crane girder fatigue life determination using S–N and LEFM methods. Engineering Failure Analysis, 79, 812-819.

[2] Zhao, Y., et al. (2022). Fatigue analysis of welded joints in crane girders. Engineering Failure Analysis, 132, 105859.

[3] Pelayo, F., Rodríguez, C., & Canteli, A. F. (2015). Failure and repair analysis of a runway beam. Engineering Failure Analysis, 56, 89-97.

[4] EN 1993-1-9:2005, Eurocode 3 – Design of steel structures – Part 1-9: Fatigue.

[5] EN 13001-3-1+A1:2013, Cranes – General design – Part 3-1: Limit states and proof of competence of steel structures.

[6] Pelayo, F., et al. (2015). Premature fatigue in crane runway girders. Engineering Failure Analysis, 56, 89-97.

[7] Domazet, Ž., Lukša, F., & Bugarin, M. (2014). Failure of two overhead crane shafts. Engineering Failure Analysis, 44, 125-135.

[8] EN 13001-3-8:2021 (Draft), Cranes – General design – Part 3-8: Shafts.

[9] Dönerkaya, A., et al. (2024). Fatigue assessment of C-type portal crane shafts. Conference Proceedings.

[10] Chen, X., et al. (2022). Improvement of fatigue strength in crane spreader structures by reinforcement plates. Int. Journal of Fatigue, 160, 106992.

[11] Pástor, M., et al. (2022). Experimental investigation of fatigue life in bridge cranes. Applied Sciences, 12(20), 10319.